Photochemical & Photobiological Sciences
https://doi.org/10.1007/s43630-024-00576-9

ORIGINAL PAPERS

Fluorescence enhancement of benzimidazolium derivative on clay nanosheets by surface-fixation induced emission (S-FIE)

Hakan Mori[1] · Ryosuke Nakazato[2] · Hiroshi Tachibana[1,3] · Tetsuya Shimada[1] · Tamao Ishida[1,3] · Miyajima Ryo[4] · Eietsu Hasegawa[4] · Shinsuke Takagi[1,3]

Received: 22 February 2024 / Accepted: 10 April 2024

Abstract

The photophysical behaviors of benzimidazolium derivative [4-(1,3-dimethylbenzimidazol-3-imu-2-yl)-*N*, *N*-diphenylaniline (2-(4-(diphenylamino)phenyl)-1,3-dimethyl-1H-benzo[d]imidazol-3-ium)] (BID) in water, organic solvents and on synthetic saponite were investigated. The fluorescence quantum yield (Φ_f) of BID was 0.91 on the saponite surface under the optimal condition, while that in water was 0.010. Such fluorescence enhancement on the inorganic surface is called "surface-fixation induced emission (S-FIE)". This fluorescence enhancement ratio for BID is significantly high compared to that of conventional S-FIE active dyes. From the values of Φ_f and the excited lifetime, the non-radiative deactivation rate constant (k_{nr}) and radiative deactivation rate constant (k_f) of BID on the saponite surface and in water were determined. Results showed that the factors for fluorescence enhancement were both the increase of k_f and the decrease of k_{nr} on the saponite surface; especially, k_{nr} decreased by more than two orders due to the effect of nanosheets.

Graphic abstract

The fluorescence quantum yield increased approximately 90 times by the addition of clay.

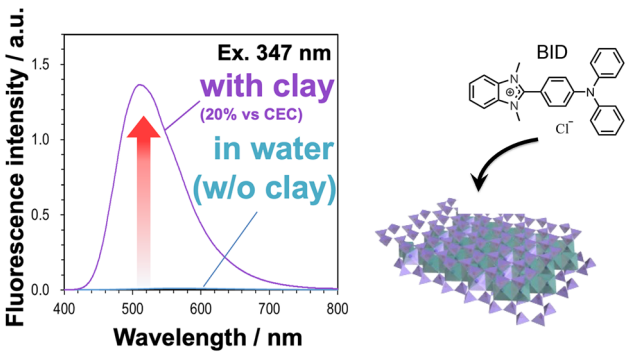

✉ Eietsu Hasegawa
ehase@chem.sc.niigata-u.ac.jp

✉ Shinsuke Takagi
takagi-shinsuke@tmu.ac.jp

[1] Department of Applied Chemistry for Environment, Graduate School of Urban Environmental Sciences, Tokyo Metropolitan University, 1-1 Minami-Ohsawa, Hachioji-Shi, Tokyo 192-0397, Japan

[2] Department of Chemistry, School of Science, Tokyo Institute of Technology, 2-12-1-NE-2 Ookayama, Meguro-Ku, Tokyo 152-8550, Japan

[3] Research Center for Hydrogen Energy-Based Society (ReHES), Tokyo Metropolitan University, 1-1 Minami-Ohsawa, Hachiohji-Shi, Tokyo 192-0397, Japan

[4] Department of Chemistry, Faculty of Science, Niigata University, Niigata 950-2181, Japan

Published online: 28 April 2024

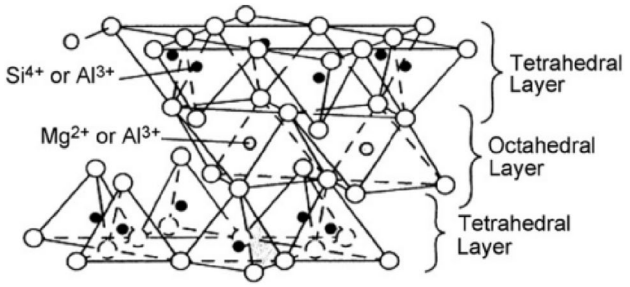

Fig. 1 The unit structure of synthetic saponite. The properties are described in "Experimental section"

1 Introduction

Layered materials are widely used for photoenergy conversion [1–4], drug delivery systems [5], and so on. They possess quite flat two-dimensional surfaces, where a variety of molecules and ions could be adsorbed through electrostatic and hydrophobic interactions [6, 7]. Furthermore, the photochemical behavior of molecules could be affected by the complex formation with layered materials [8–30]. Among the layered materials, synthetic saponite type of clay minerals (Fig. 1) are frequently used as host materials, because they possess appropriate anionic charge density in the structure for exfoliation in water [31]. When saponite nanosheets exfoliate in water, the available surface area increases, and the solution is substantially transparent; thus, they are fascinating materials from a viewpoint of surface and photochemistry [32]. Our group has reported the unique photophysical properties of the hybrids composed of saponite and cationic dyes such as porphyrins, sub-porphyrins, and triphenyl benzene dyes [33–35]. By using size-matching effect [36, 37], it was reported that high-density adsorption assembly of dyes without an aggregation on the clay surface that can be available for the construction of artificial photosynthesis systems [38–40] was attained. In addition, by the adsorption on saponite, the emission enhancement behavior of molecules on the clay surface compared with that in bulk water was found out. Such emission enhancement behavior is called surface-fixation induced emission (S-FIE) [35, 41–45]. As an emission enhancement behavior, aggregation-induced emission (AIE) has been widely investigated [46–50]. Compared to AIE, S-FIE has some advantages: (1) S-FIE does not need organic solvents, (2) it is easy to know whether emission enhancement of molecule will be induced or not, and (3) the emission enhancement mechanism is relatively clear. In addition, clay minerals are environmentally friendly. Thus, the dye–clay composites could be promising for the construction of photofunctional materials.

In this study, we focused on [4-(1,3-dimethylbenzimidazol-3-imu-2-yl)-*N*, *N*-diphenylaniline (2-(4-(diphenylamino)phenyl)-1,3-dimethyl-1H-benzo[d]imidazol-3-ium)] (BID, Fig. 2) as a guest molecule on the clay surface. The emission enhancing behavior and the photophysical properties of BID on the clay surface were investigated in detail. Unique photophysical and redox properties of BID have been reported by Hasegawa et al. [51]. Because BID possesses a cationic part and aromatic rings in its molecular structure, it is expected that BID could be adsorbed on the clay surface by electrostatic and hydrophobic interactions. When BID is adsorbed on the clay surface, it is expected that the molecular structure becomes planar compared to that in bulk solution, and the intramolecular motion is suppressed. Because BID possesses rotatable bonds and non-planar parts, the molecular structure, intramolecular motion, and thus the photophysical properties are affected by adsorption onto the clay surface. So far, we have reported the behavior of S-FIE with porphyrazine, triphenylbenzene, acridinium, hemicyanine, and phenanthridine derivatives, and so on [35, 41–45]. This is the first report on the adsorption and emission behavior of benzimidazolium derivatives onto saponite clay surface. Eventually, a remarkable emission enhancement for BID was discovered, and the mechanism for the emission enhancement was discussed.

2 Experimental section

2.1 Materials

Sumecton SA (denoted as SSA) as a synthetic saponite was received from Kunimine Industries Co., Ltd. and was used without further purification. The stoichiometric formula of SSA is $[(Si_{7.20}Al_{0.80})(Mg_{5.97}Al_{0.03})O_{20}(OH)_4]^{-0.77}(Na_{0.49}Mg_{0.14})^{+0.77}$. The cation exchange capacity (CEC) of the saponite is *ca.* 1.0×10^{-3} equiv. g^{-1}. The average

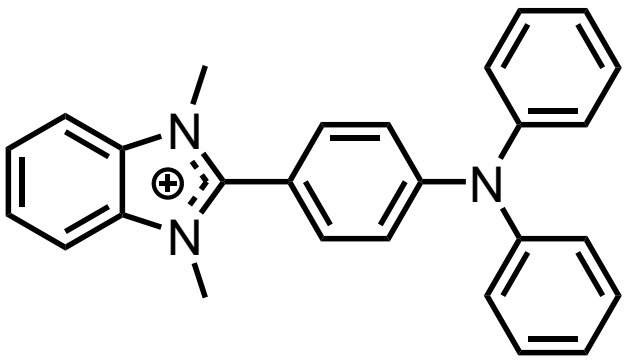

Fig. 2 The structure of [4-(1,3-dimethylbenzimidazol-3-imu-2-yl)-*N*, *N*-diphenylaniline (2-(4-(diphenylamino)phenyl)-1,3-dimethyl-1H-benzo[d]imidazol-3-ium)] (BID)

distance between the anionic points on the saponite surface is estimated to be 1.2 nm, on the basis of the assumption of a hexagonal array. The aqueous dispersion of saponite nanosheet whose particle size is small (<100 nm) is substantially transparent in the UV–visible range. The synthesis procedure of [4-(1,3-dimethylbenzimidazol-3-imu-2-yl)-*N*, *N*-diphenylaniline (2-(4-(diphenylamino)phenyl)-1,3-dimethyl-1H-benzo[d]imidazol-3-ium)] (BID) (denoted as BID) has been described in a previous paper [51] and the counter anion was exchanged to Cl^- from ClO_4^- by the use of ion-exchange resin (Organo, Amberlite Resin IRA-400).

2.2 Analysis

UV–visible absorption spectra were obtained on Shimadzu UV-3150 spectrophotometer. Fluorescence spectra were recorded on JASCO FP-6600 spectrofluorometer. The value of quantum yields was measured on Hamamatsu Photonics C13534-01 UV–NIR absolute PL quantum yield spectrometer. Time-resolved fluorescence signals were measured by Hamamatsu Photonics C4780 detector system based on a streak camera. Nd^{3+} YAG laser was used for excitation. TG/DTA curves were measured with a Shimadzu DTG-60H analyzer to determine the water content of SSA.

2.3 Sample preparation for the analysis of adsorption behavior

UV–Vis absorption spectra of BID in aqueous SSA dispersion were measured under the concentration of BID = 10–130% vs CEC of SSA to discuss the adsorption behavior of BID onto the clay surface. First, a total volume 3100 µL of the sample [(SSA) = 3.23×10^{-5} eq L^{-1}] was prepared in a quartz cell (1.0 × 1.0 cm). Then, by adding to the sample 20 µL of the BID stock solution, whose concentration was 1.0×10^{-4} M, samples with concentration ratios of (BID)/(SSA) = 10, 20, 30, 40, 50, 60, 70, 80, 90, 100, 110, 120, and 130% vs CEC were obtained.

2.4 Sample preparation for steady-state spectroscopic measurements.

To measure UV–Vis absorption and fluorescence spectra of BID in water, organic solvents, and SSA dispersion (20% vs CEC), sample preparation was performed to have an absorbance of approximately 0.05 to keep the linearity of absorbance and emission intensity. The fluorescence spectra were corrected for the absorbed light amount at the excitation wavelength. Typical conditions are as follows: (BID) = 3.85×10^{-6} M and 2.67×10^{-6} M in the water sample and in the organic solvent samples, respectively. A sample of BID in SSA aqueous dispersion (20% vs CEC) was prepared in a quartz cell [(SSA) = 1.92×10^{-5} eq L^{-1}, (BID) = 3.85×10^{-6} M].

2.5 Sample preparation for fluorescence quantum yield measurements

The sample of BID in water or organic solvent was prepared in a quartz cell and the fluorescence quantum yield was measured. Typical conditions are as follows; (BID) = 1.61×10^{-5} M and 8.00×10^{-6} M in water sample and in organic solvent samples, respectively. The sample of BID in SSA aqueous dispersion (20% vs CEC) was prepared in a quartz cell and the value of fluorescence quantum yield measured [(SSA) = 1.92×10^{-5} eq L^{-1}, (BID) = 3.85×10^{-6} M]. The value of fluorescence quantum yield for BID was determined by the absolute method using Hamamatsu Photonics C13534-01 UV–NIR absolute PL quantum yield spectrometer.

2.6 Sample preparation for time-resolved spectroscopic measurements

A sample of BID in water or organic solvent was prepared in a quartz cell and the excited-state lifetime was measured. Typical conditions are as follows: (BID) = 1.61×10^{-5} M and 8.00×10^{-6} M in water sample and in organic solvent samples, respectively. A sample of BID in SSA aqueous dispersion (20% vs CEC) was prepared in a quartz cell and the excited lifetime was measured [(SSA) = 1.85×10^{-5} eq L^{-1}, (BID) = 3.70×10^{-6} M] by a C4780 picosecond fluorescence lifetime measurement system (Hamamatsu Photonics). Nd^{3+} YAG laser (EKSPLA PL2210JE + PG-432, fwhm 25 ps, 1 kHz) was used for excitation. The excitation wavelength was 355 nm. The fluorescence lifetimes were calculated by deconvoluting the excitation pulse in each measurement range.

3 Results and discussion

3.1 Absorption behavior of BID in water and on the clay surface

The adsorption behavior of BID onto the clay surface was observed by UV–Vis absorption measurements. The absorption spectra of BID without and with SSA in aqueous solution are shown in Fig. 3. As described later, BID molecule does not form aggregates on the SSA surface under the present conditions.

The λ_{max} of BID was shifted to longer wavelength by the adsorption on SSA compared to that in water. Such shift of λ_{max} has been reported for an adsorbed molecule on the clay surface [10, 11, 13, 21, 29, 31]. This phenomenon is

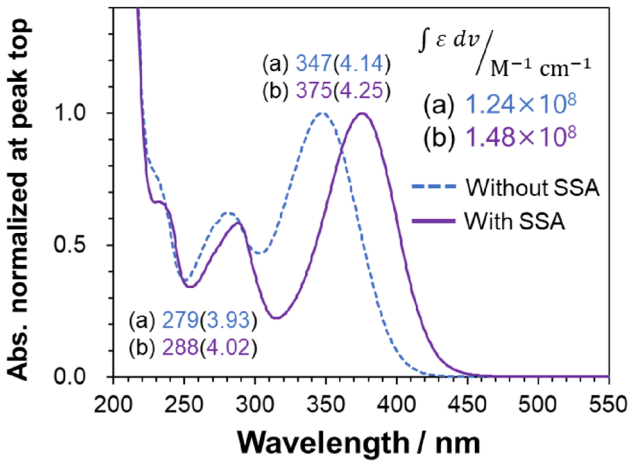

Fig. 3 UV–Vis absorption spectra of BID **a** without and **b** with SSA in aqueous solution. **a** (BID) = 9.80 × 10^{-6} M in water and **b** (BID) = 3.30 × 10^{-5} M (=30% vs CEC) and (SSA) = 1.10 × 10^{-4} equiv. L^{-1} in water. The maxima wavelength of absorption $\lambda_{abs.}$/nm (extinction coefficient, log $\varepsilon_{max.}$) and the value of integral of the extinction coefficient $\int\varepsilon\, d\nu$ [22,222–40,000 cm^{-1} (250–450 nm)] are shown in Fig. 3.

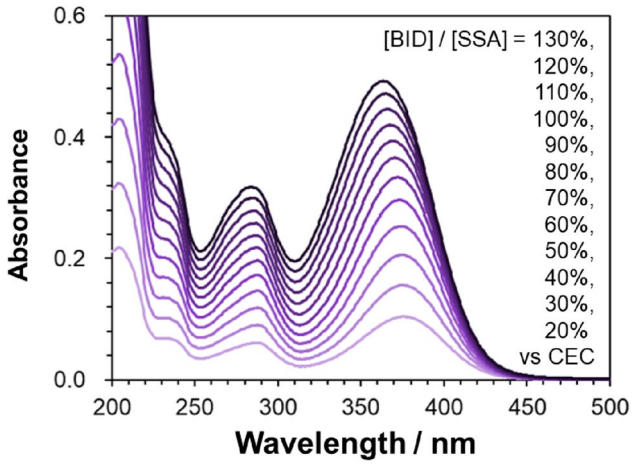

Fig. 4 UV–Vis absorption spectra of BID on clay for 20, 30, 40, 50, 60, 70, 80, 90, 100, 110, 120, and 130% vs CEC in aqueous solution. (BID) = 0.64–3.87 × 10^{-5} M (=20–130% vs CEC) and (SSA) = 2.98–3.23 × 10^{-5} equiv. L^{-1} in water

proposed to be caused by the expansion of the π-conjugated system due to the adsorption of dye molecules onto the atomically flat clay surface [52–54]. Because BID possesses rotatable aromatic parts in the molecule, the λ_{max} shift of BID could be rationalized along with the previously proposed mechanism. In addition, the integral of extinction coefficient [250–450 nm (22,222–40,000 cm^{-1})] of BID was increased by 1.2 times by the adsorption onto the SSA surface. This phenomenon indicates that the transition probability of BID was increased by the adsorption onto the SSA surface. The increase in transition probability could be induced by an increase in the Franck–Condon factor resulting from the similarization in molecular structures between the ground and excited states. The details will be discussed later.

3.2 Adsorption behavior of BID on the clay surface

The absorption spectra of BID on the SSA surface, where the loading level of BID is 20–130% vs CEC of the clay, are shown in Fig. 4.

Judging from the normalized spectra (Figure S1), the absorption spectral shape is same under the loading level of 20–40% vs CEC. This indicates that all BID molecule was adsorbed on the SSA surface, and there was no interaction between the transition dipole moments of BID under the conditions. In other word, BID does not form aggregates below 40% adsorption vs CEC. Above 40% loadings, as the loading level of BID increased, the spectrum was shifted to shorter wavelength. The spectrum of non-adsorbed BID was superimposed above 40% loadings.

All absorption spectrum in Fig. 4 can be expressed by the linear combination of the spectrum of adsorbed and non-adsorbed BID as shown in Figure. S2. By this fitting procedure, the adsorption amount of BID was determined for each loading level. The adsorption behavior was analyzed according to Langmuir isotherm. The adsorption equilibrium can be expressed by Eqs. 1 and 2.

$$\text{BID} + \text{SSA} \rightleftharpoons \text{BID - SSA complex}, \tag{1}$$

$$\frac{q}{q_{max}} = \frac{KC}{1+KC}, \tag{2}$$

where q is the adsorption amount (μmol g^{-1}), q_{max} is the maximum adsorption amount, C (M) is (BID) in bulk aqueous solution, and K (M^{-1}) is the equilibrium constant between BID and SSA.

Langmuir adsorption isotherm plot is shown in Fig. 5. The plots were well fitted with Eq. 2 as can be seen in the figure. This indicates that the present system fulfills the assumption that (1) the adsorption is a monolayer at the surface; (2) there is no interaction between molecules on different sites; (3) the adsorption is equal for all sites. By the Langmuir analysis, q_{max} and K were determined to be 61% vs CEC and 1.9 × 10^6 M^{-1}, respectively. It is known that multi-cationic molecules that fulfill the size-matching rule do not form aggregates on the SSA surface [33–40]. On the other hand, mono-cationic molecules tend to form aggregates [37], and thus the non-aggregation behavior of BID on the SSA surface is a unique phenomenon. It is assumed that bulky non-planar molecular structure of BID could suppress the formation of aggregates. Because the formation of aggregates makes the photophysical behavior complicated, the adsorption behavior of BID without

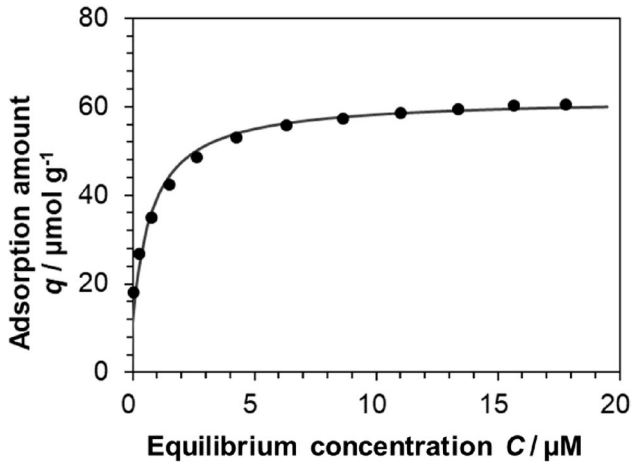

Fig. 5 Langmuir isotherm plot (plot of the adsorption amount of BID on the clay with respect to the equilibrium concentration of BID), (BID) = 0.64–3.87 × 10^{-5} M (=20–130% vs CEC) and (SSA) = 2.98–3.23 × 10^{-5} equiv. L^{-1} in water

aggregation is beneficial from the viewpoint of photophysical analysis.

3.3 Fluorescence behavior of BID in water and on the clay surface

The fluorescence behavior of BID on the SSA surface was analyzed by steady-state and time-resolved fluorescence measurements. The fluorescence spectra of BID with and without SSA under the typical conditions are shown in Fig. 6a. As can be seen, a remarkable increase of fluorescence of BID by the adsorption onto the SSA surface was observed. The fluorescence quantum yields (Φ_f) of BID without and with SSA are 0.010 and 0.69, respectively. The coverage of BID onto the SSA is 20% vs CEC, and 69 times increase of fluorescence was observed. Thus, it was found out that BID is an S-FIE active dye. The observed high fluorescence enhancement ratio by the adsorption could be attributed to the molecular structure of BID that has many rotatable parts in the molecule. As can be seen in Fig. 6b, the emission maximum wavelength was shifted from 567 to 510 nm by the adsorption onto the SSA surface. Because the absorption maximum was shifted to longer wavelength (see Fig. 3) by the adsorption, the Stokes shift for BID on the SSA surface was decreased compared with that in bulk water. Stokes shift is a clue for the discussion on the mechanism of fluorescence enhancement. The discussion on the fluorescence enhancement of BID on the SSA surface is described later.

For further detailed discussions, the fluorescence decay curves (the scale of fluorescence intensity is logarithmic) for BID with and without SSA are shown in Fig. 7. Raw

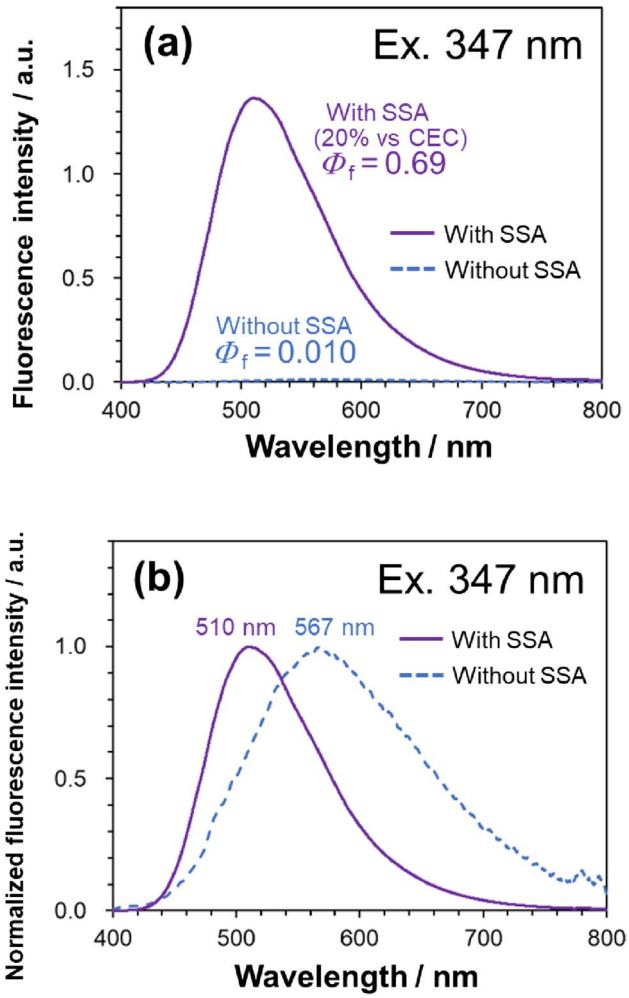

Fig. 6 **a** Steady-state fluorescence spectra of BID, **b** normalized steady-state fluorescence spectra of BID at the peak top, with and without clay in water [(BID) = 3.85 × 10^{-6} M in water sample, and (BID) = 3.85 × 10^{-6} M (=20% vs CEC) and (SSA) = 1.92 × 10^{-5} equiv. L^{-1} in SSA aqueous solution]. The excitation wavelength was 347 nm. The spectra in **a** were corrected with the absorbance at 347 nm. The value of fluorescence quantum yield and maximum wavelength of fluorescence are shown in Fig. 6.

fluorescence decay curves of BID are shown in Figure S3. Both decay curves were straight and can be analyzed by a single component decay. The obtained excited lifetime (τ) of BID without and with SSA (20% vs CEC) is 0.12 and 3.2 ns, respectively. This single component decay also supports that BID does not form aggregates on the SSA surface.

By using the value of the fluorescence quantum yield (Φ_f) and the excited lifetime (τ), the photophysical parameters such as a radiative deactivation rate constant (k_f) and a non-radiative deactivation rate constant (k_{nr}) can be calculated, according to Eqs. 3 and 4. The obtained photophysical parameters are summarized in Table 1.

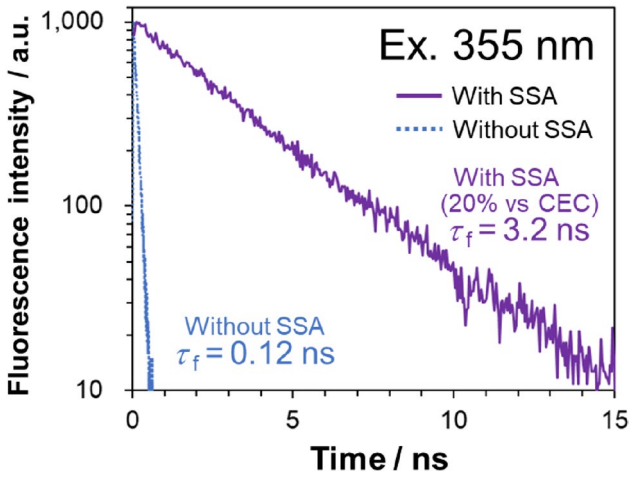

Fig. 7 Fluorescence decay curves of BID (the scale of fluorescence intensity is logarithmic) with and without SSA in water [(BID) = 1.61×10^{-5} M in water sample, and (BID) = 3.70×10^{-6} M (=20% vs CEC) and (SSA) = 1.85×10^{-5} equiv. L^{-1} in SSA aqueous solution]. The excitation wavelength was 355 nm. The value of fluorescence lifetime is shown in the figure. The raw decay curves are shown in Figure S3

Table 1 Photophysical parameters of BID with and without SSA

Condition	Fluorescence quantum yield	Fluorescence lifetime/ns	k_f/s^{-1}	k_{nr}/s^{-1}
Water (without SSA)	0.010	0.12	8.3×10^7	8.3×10^9
SSA aq. (20% vs CEC)	0.69	3.2	2.2×10^8	9.7×10^7

$$k_f = \frac{\Phi_f}{\tau}, \tag{3}$$

$$k_{nr} = \frac{1 - \Phi_f}{\tau}, \tag{4}$$

$$\Phi_f = \frac{k_f}{k_f + k_{nr}}. \tag{5}$$

The fluorescence quantum yield (Φ_f) is expressed in Eq. 5. Thus, it was shown that the fluorescence enhancement on the SSA surface was governed by both an increase in k_f and a decrease in k_{nr}. It should be noted that the suppression of k_{nr} by two orders of magnitude is significantly larger compared to conventional S-FIE [34, 35, 41, 42, 44, 45]. This could be attributed to the molecular structure of BID that has many rotatable parts in the molecule.

To make the effects of the SSA surface clear, the photophysical behavior of BID was observed in various organic solvents. The fluorescence decay curves and spectra are shown in Figure S4 and S5. In addition, the absorption spectra and the λ_{max} are shown in Figure S6 and Table S1. The obtained photophysical parameters are shown in Table 2.

As can be seen in Table 2, the effects of SSA on the photophysical parameters of BID are outstanding compared to other solvents. In contrast to BID on SSA, the values of k_f for BID are almost the same as in water and in organic solvents. In addition, the value of k_{nr} for BID adsorbed on SSA is minimal compared with that in other bulk solvents. These results indicate that BID adsorbed on the clay surface exhibits its unique photophysical properties which are not observed in bulk solution.

3.4 Effects of SSA concentration on the fluorescence behavior of BID

The fluorescence quantum yield (Φ_f) of BID was measured at various concentrations of SSA (4.98×10^{-6} to 9.95×10^{-4} equiv. L^{-1}). The concentration of BID was constant (4.98×10^{-7} M), and the adsorption density of BID was 0.05 ~10% vs CEC. The λ_{max} for absorption and fluorescence, the Stokes shift, and Φ_f are summarized in Table 3. The absorption and fluorescence spectra are shown in Figure S7, the photograph of samples is shown in Fig. 8, and the fluorescence spectra of BID with the value of Φ_f is shown in Figure S8.

As the concentration of SSA increased, the value of Stokes shift decreased and Φ_f increased. In general, as the concentration increased, clay nanosheet tends to form stacked structure, while it exfoliates into a single layer at low concentration condition in water [36]. In addition, it was reported that the absorption λ_{max} was further shifted to longer wavelength when the dye was intercalated by clay nanosheets, compared to that on exfoliated clay nanosheets [36, 55]. Taking these facts into account, it is expected

Table 2 The value of fluorescence quantum yield (Φ_f), fluorescence lifetime (τ), and deactivation rate constant (k_f and k_{nr}) of BID in water and various organic solvents

Solvent	Fluorescence quantum yield	Fluorescence lifetime/ns	k_f/s^{-1}	k_{nr}/s^{-1}
Water	0.010	0.12	8.3×10^7	8.3×10^9
Methanol	0.052	0.67	7.8×10^7	1.4×10^9
Ethanol	0.093	1.05	8.9×10^7	8.6×10^8
1-Propanol	0.14	1.59	8.7×10^7	5.4×10^8
DMSO	0.049	0.63	7.3×10^7	1.4×10^9
Acetone	0.055	0.79	7.0×10^7	1.2×10^9
Acetonitrile	0.066	0.85	7.8×10^7	1.1×10^9
SSA aq. (20% vs CEC)	0.69	3.20	2.2×10^8	9.7×10^7

Table 3 The value of maximum wavelength, Stokes shift, and fluorescence quantum yield (Φ_f) of BID on SSA surface at different SSA concentrations

Concentration of SSA/equiv. L^{-1}	Loading level of BID	Maximum wavelength of absorption/nm	Maximum wavelength of fluorescence/nm	Stokes shift/cm^{-1}	Φ_f
4.98×10^{-6}	10% vs CEC	376	510	6988	0.72
9.95×10^{-6}	5% vs CEC	376	505	6794	0.73
4.98×10^{-5}	1% vs CEC	388	503	5892	0.76
9.95×10^{-5}	0.5% vs CEC	392	505	5708	0.82
4.98×10^{-4}	0.1% vs CEC	391	493	5291	0.87
9.95×10^{-4}	0.05% vs CEC	392	491	5144	0.91

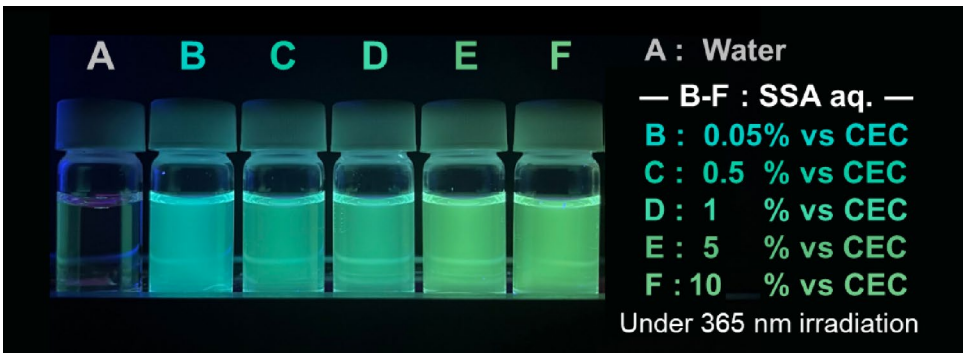

Fig. 8 Photograph of the SSA–BID complexes at different SSA concentrations on black light (365 nm). (BID) = 4.98×10^{-7} M

Table 4 The value of fluorescence quantum yield (Φ_f) before and after a freeze–thaw treatment of BID on SSA at different concentrations of SSA

Concentration of SSA/equiv. L^{-1}	Loading level of BID	Fluorescence quantum yield	
		Before freeze–thaw	After freeze–thaw
9.95×10^{-6}	5% vs CEC	0.73	0.81
9.95×10^{-5}	0.5% vs CEC	0.82	0.85
9.95×10^{-4}	0.05% vs CEC	0.91	0.90

that Φ_f can be further increased by the intercalation of BID between the SSA nanosheets. It was reported that stacked structures of clay nanosheets can be prepared by a freeze–thaw treatment of the sample [36]. To confirm the hypothesis that Φ_f was increased by the intercalation of BID, the effect of a freeze–thaw treatment on the fluorescence behavior was examined for the sample where the SSA concentration was 9.95×10^{-6}, 9.95×10^{-5}, 9.95×10^{-4} equiv. L^{-1} (loading level is 5, 0.5, and 0.05% vs CEC). The values of Φ_f before and after freeze–thaw treatments are summarized in Table 4.

For the sample where the concentration of SSA is 9.95×10^{-6} and 9.95×10^{-5} equiv. L^{-1}, Φ_f was increased by a freeze–thaw treatment. On the other hand, Φ_f was not affected by a freeze–thaw treatment for the sample where the concentration of SSA was 9.95×10^{-4} equiv. L^{-1}. The photograph of the samples is shown in Figure S9, and the normalized steady-state fluorescence spectra of the BID–SSA complex at concentration of SSA 9.95×10^{-6} equiv. L^{-1} before and after a freeze–thaw are shown in Figure S10. As can be seen in Figure S10, the fluorescence λ_{max} was shifted to shorter wavelength by a freeze–thaw treatment. This blue shift is similar to the effects of fluorescence behavior for BID under the high SSA concentration conditions. These results indicate that the reason for the increase of $_f$ by the increase of SSA concentration is the formation of stacked structure of SSA nanosheets. When the concentration of SSA is 9.95×10^{-4} equiv. L^{-1}, all SSA nanosheets are stacked and all BID molecules are intercalated. For the sample where the concentration of SSA is 9.95×10^{-5} equiv. L^{-1}, both exfoliated and stacked SSA nanosheets coexist in the sample solution. It is reasonable that the intramolecular motion, which leads to non-radiative deactivation, is more suppressed in the stacked structure, compared to the exfoliated condition. Because a highest Φ_f was obtained when the SSA concentration was 9.95×10^{-4} equiv. L^{-1}, the fluorescence lifetime was measured at the condition (Figure S11), and the value of k_f and k_{nr} was calculated for the sample where the SSA concentration was 9.95×10^{-4} equiv. L^{-1}. The fluorescence decay curve can be analyzed by a single component. This supports that all the SSA nanosheets completely form stacked structures at the concentration of 9.95×10^{-4} equiv. L^{-1}. Under the condition, k_f and k_{nr} were

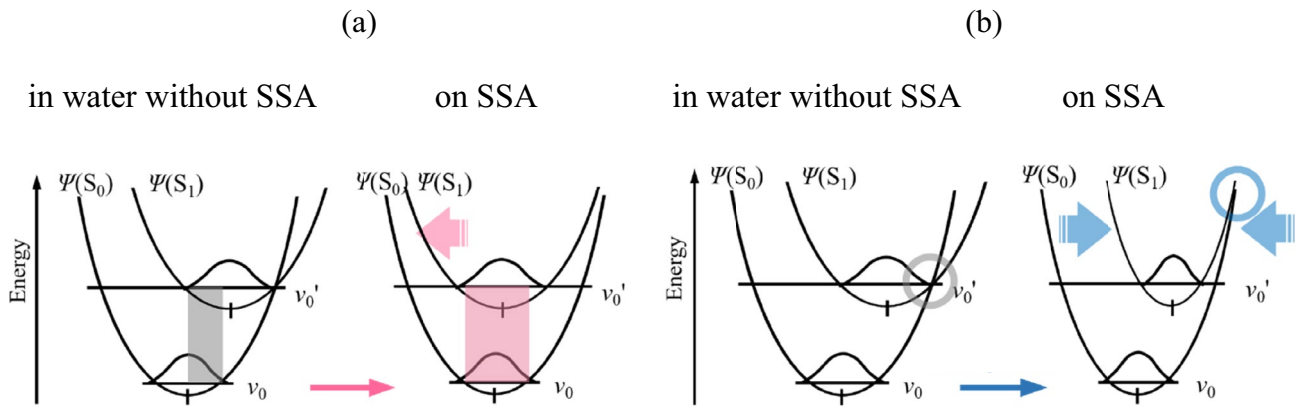

Fig. 9 Plausible conceptual potential energy curves of ground and excited states for BID. **a** Structure resembling effect. **b** Structure fixing effect

calculated to be 2.6×10^8 s^{-1} and 2.6×10^7 s^{-1}, respectively. The highest Φ_f and the longest fluorescence lifetime of BID in the present study were 0.91 and 3.51 ns, respectively.

3.5 Mechanism of fluorescence enhancement of BID on the SSA surface

For the BID molecule, the values of k_f and k_{nr} were increased and decreased, respectively, by the adsorption onto the SSA nanosheet, compared to those in water or organic solvents. Along with the previous reports [56], these effects of the SSA nanosheet could be explained by the use of potential energy surface. The plausible conceptual potential energy curves of the ground and excited states for BID are shown in Fig. 9. Figure 9 shows the effect of clay surface on the potential energy surface for the adsorbed molecule; (a) on SSA, the most stable structure is relatively similar between the ground and excited states, compared to that in water without SSA (structure resembling effect [56]). Because Franck–Condon factor increased by the adsorption onto SSA, k_f could be increased. (b) On SSA, the potential energy curve was relatively sharpened against the nuclear coordinates, compared to that in water without SSA (structure fixing effect [56]). Because of the increase of activation energy for the process from S_1 to high vibrational state of S_0 (indicated by circle in Fig. 9 (b)) by the adsorption onto the SSA surface, k_{nr} is decreased. In this study, by the adsorption onto the SSA surface, the following were observed for BID: (1) the absorption λ_{max} shifts to longer wavelength, (2) the fluorescence λ_{max} shifts to shorter wavelength, (3) the absorption coefficient increases, (4) k_f increases, and (5) k_{nr} decreases. All these observations are consistent to the proposed mechanism shown in Fig. 9. As a conclusion, Φ_f of BID was increased both by the increase of k_f and the decrease of k_{nr}. As can be seen in Tables 2 and 5, the decrease of k_{nr} is the major factor for the increase of Φ_f. By the intercalation of BID between the SSA nanosheets, the decrease of k_{nr} and the increase of Φ_f were further enhanced. It was indicated that the effect of fixation of molecule on the SSA surface on the photophysical parameters, especially for $k_{nr,}$ is significant for the molecule having many rotatable parts.

4 Conclusion

In this study, the photophysical properties of BID on the SSA surface, in water, and in organic solvents, were investigated. The fluorescence quantum yield ($_f$) of BID was much enhanced when BID was adsorbed on the SSA surface. Φ_f was further enhanced when BID was intercalated between the SSA nanosheets. While Φ_f in water was 0.010, that with clay was 0.91 when BID was intercalated. The photophysical parameters such as k_f and k_{nr} were calculated from the value of $_f$ and τ. The enhancement of Φ_f is attributed to both the increase of k_f and the decrease of k_{nr}. For BID having many rotatable parts, the suppression of k_{nr} was remarkable. These results indicate that the effect of molecular fixation on the clay surface could be more effective for the molecule that has many rotatable parts in the molecule.

Supplementary Information The online version contains supplementary material available at https://doi.org/10.1007/s43630-024-00576-9.

Funding Open access funding provided by Tokyo Metropolitan University. Japan Society for the Promotion of Science, JP22K19090, Shinsuke Takagi.

Declarations

Conflict of interest The authors declare no completing financial interest.

References

1. Ishida, Y., Shimada, T., Masui, D., Tachibana, H., Inoue, H., & Takagi, S. (2011). Efficient excited energy transfer reaction in clay/porphyrin complex toward an artificial light-harvesting system. *Journal of the American Chemical Society, 133*, 14280–14286.
2. Ohtani, Y., Shimada, T., & Takagi, S. (2015). Artificial light-harvesting system with energy migration functionality in a cationic dye/inorganic nanosheet complex. *Journal of Physical Chemistry C, 119*, 18896–18902.
3. Tsukamoto, T., Ramasamy, E., Shimada, T., & Takagi, S. (2016). Supramolecular surface photochemistry: Cascade energy transfer between encapsulated dyes aligned on a clay nanosheet surface. *Langmuir, 32*, 2920–2927.
4. Ohtani, Y., Kawaguchi, S., Shimada, T., & Takagi, S. (2017). Energy transfer among three dye components in a nanosheet-dye complex: An approach to evaluating the performance of a light-harvesting system. *Journal of Physical Chemistry C, 121*, 2052–2058.
5. Aisawa, S., Sang, J., Suga, D., Hirahara, H., & Narita, E. (2022). Preparation of hollow nanosphere of 5-fluorouracil/layered double hydroxide and its cellular cytotoxicity. *Applied Clay Science, 226*, 106575.
6. Ogawa, M., & Kuroda, K. (1995). Photofunctions of intercalation compounds. *Chemical Reviews, 95*, 399–438.
7. Grabolle, M., Starke, M., & Resch-Genger, U. (2016). Highly fluorescent dye-nanoclay hybrid materials made from different dye classes. *Langmuir, 32*, 3506–3513.
8. Takagi, K., & Shichi, T. (2000). Clay minerals as photochemical reaction fields. *Journal of Photochemistry and Photobiology. A: Photochemical Reviews, 1*, 113–130.
9. Bujdak, J., & Komadel, P. (1997). Interaction of methylene blue with reduced charge montmorillonite. *The Journal of Physical Chemistry B, 101*, 9065–9068.
10. Arbeloa, F. L., Martínez, V. M., Arbeloa, T., & Arbeloa, I. L. (2007). Photoresponse and anisotropy of rhodamine dye intercalated in ordered clay layered films. *Journal of Photochemistry and Photobiology C, 8*, 85–108.
11. Čeklovský, A., Czímerová, A., Pentrák, M., & Bujdák, J. (2008). Spectral properties of TMPyP intercalated in thin films of layered silicates. *Journal Colloid and Interface Science, 324*, 240–245.
12. Zhou, C. H., Shen, Z. F., Liu, L. H., & Liu, S. M. (2011). Preparation and functionality of clay-containing films. *Journal of Materials Chemistry, 21*, 15132–15153.
13. Bergaya, F., & Van Damme, H. (1982). Stability of metalloporphyrins adsorbed on clays: A comparative study. *Geochimica et Cosmochimica Acta, 46*, 349–360.
14. Podsiadlo, P., Shim, B. S., & Kotov, N. A. (2009). Polymer/clay and polymer/carbon nanotube hybrid organic-inorganic multilayered composites made by sequential layering of nanometer scale films. *Coordination Chemistry Reviews, 253*, 2835–2851.
15. Carrado, K. A. (2000). Synthetic organo- and polymer-clays: Preparation, characterization, and materials applications. *Applied Clay Science, 17*, 1–23.
16. Theng, B. K. G. (2012). Formation and properties of clay-polymer complexes. *Developments in Clay Science, 4*, 201–241.
17. Liu, P. (2007). Polymer modified clay minerals: A review. *Applied Clay Science, 38*, 64–76.
18. Choy, J. H., Choi, J. M., Oh, J. M., & Park, T. (2007). Clay minerals and layered double hydroxides for novel biological applications. *Applied Clay Science, 36*, 122–132.
19. Ruiz-Hitzky, E., Aranda, P., Darder, M., & Ogawa, M. (2010). Hybrid materials based on clays for environmental and biomedical applications. *Journal of Materials Chemistry*, *20*, 9306–9321.
20. Fukushima, Y. (2005). Organic/inorganic interactions in polymer/clay mineral hybrids. *Clay Science, 12*, 79–82.
21. Okada, T., Ide, Y., & Ogawa, M. (2012). Organic–inorganic hybrids based on ultrathin oxide layers: Designed nanostructures for molecular recognition. *Chemistry Asian Journal, 7*, 1980–1992.
22. Ruiz-Hitzky, E., Aranda, P., Darder, M., & Ogawa. M. Hybrid and biohybrid silicate based materials: Molecular vs. block-assembling bottom-up processes. *Chemistry Society Reviews, 40*, 801–828.
23. Chakraborty, C., Dana, K., & Malik, S. (2011). Intercalation of perylenediimide dye into LDH clays: Enhancement of photostability. *Journal of Physical Chemistry C, 115*, 1996–2004.
24. Bizaia, N., Faria, E. H. D., Ricci, G. P., Calefi, P. S., Nassar, E. J., Castro, K. A. D. F., Nakagaki, S., & Korili, S. A. (2009). Porphyrin–kaolinite as efficient catalyst for oxidation reactions. *ACS Applied Materials & Interfaces, 1*, 2667–2678.
25. Čeklovský, A., Czímerová, A., Lang, K., & Bujdák, J. (2009). Layered silicate films with photochemically active porphyrin cations. *Pure and Applied Chemistry, 81*, 1385–1396.
26. Sasai, R., Itoh, T., Ohmori, W., Itoh, H., & Kusunoki, M. (2009). Preparation and characterization of rhodamine 6G/alkyltrimethylammonium/laponite hybrid solid materials with higher emission quantum yield. *Journal of Physical Chemistry C, 113*, 415–421.
27. Yui, T., Kameyama, T., Sasaki, T., Torimoto, T., & Takagi, K. (2007). Pyrene-to-porphyrin excited singlet energy transfer in LBL-deposited LDH nanosheets. *Journal of Porphyrins and Phthalocyanines, 11*, 428–433.
28. Czímerová, A., Jankovič, L., Madejová, J., & Čeklovský, A. (2013). Unique photoactive nanocomposites based on rhodamine 6G/polymer/montmorillonite hybrid systems. *Journal of Polymer Science: Part A, 51*, 1672–1679.
29. Villemure, G., Detellier, C., & Szabo, A. G. (1986). Fluorescence of clay-intercalated methylviologen. *Journal of the American Chemical Society, 108*, 4658–4659.
30. Villemure, G., Detellier, C., & Szabo, A. G. (1991). Fluorescence of methylviologen intercalated into montmorillonite and hectorite aqueous suspensions. *Langmuir, 7*, 1215–1221.
31. Schoonheydt, R. A., De Pauw, P., Vliers, D., & De Schrijver, F. C. (1984). Luminescence of tris(2,2'-bipyridine)ruthenium(II) in aqueous clay minerals suspensions. *Journal of Physical Chemistry, 88*, 5113–5118.
32. Suzuki, Y., Tenma, Y., Nishioka, Y., & Kawamata, J. (2012). Efficient nonlinear optical properties of dyes confined in interlayer nanospaces of clay minerals. *Chemistry—An Asian Journal, 7*, 1170–1179.
33. Eguchi, M., Shimada, T., Tryk, D. A., Inoue, H., & Takagi, S. (2013). Role of hydrophobic interaction in controlling the orientation of dicationic porphyrins on solid surfaces. *Journal of Physical Chemistry C, 117*, 9245–9251.
34. Tsukamoto, T., Shimada, T., & Takagi, S. (2016). Photophysical properties and adsorption behaviors of novel tri-cationic

boron(III) subporphyrin on anionic clay surface. *ACS Applied Materials & Interfaces, 8*, 7522–7528.
35. Tsukamoto, T., Shimada, T., & Takagi, S. (2013). Unique photochemical properties of *p*-substituted cationic triphenylbenzene derivatives on a clay layer surface. *Journal of Physical Chemistry C, 117*, 2774–2779.
36. Takagi, S., Shimada, T., Eguchi, M., Yui, T., Yoshida, H., Tryk, D. A., & Inoue, H. (2002). High-density adsorption of cationic porphyrins on clay layer surfaces without aggregation: The size-matching effect. *Langmuir, 18*, 2265–2272.
37. Egawa, T., Watanabe, H., Fujimura, T., Ishida, Y., Yamato, M., Masui, D., Shimada, T., Tachiana, H., Yoshida, H., Inoue, H., & Takagi, S. (2011). Novel Methodology to control the adsorption structure of cationic porphyrins on the clay surface using the "size-matching rule." *Langmuir, 27*, 10722–10729.
38. Tatsumi, D., Tsukamoto, T., Honna, R., Hoshino, S., Shimada, T., & Takagi, S. (2017). Highly selective photochemical epoxidation of cyclohexene sensitized by Ru(II) porphyrin–clay hybrid catalyst. *Chemistry Letters, 46*, 1311–1314.
39. Ishida, Y., Shimada, T., Tachibana, H., Inoue, H., & Takagi, S. (2012). Regulation of the collisional self-quenching of fluorescence in clay/porphyrin complex by strong host-guest interaction. *Journal of Physical Chemistry A, 116*, 12065–12072.
40. Takagi, S., Shimada, T., Ishida, Y., Fujimura, T., Masui, D., Tachibana, H., Eguchi, M., & Inoue, H. (2013). Size matching effect on inorganic nanosheets: Control of distance, alignment, and orientation of molecular adsorption as a bottom-up methodology for nanomaterials. *Langmuir, 29*, 2108–2119.
41. Ishida, Y., Shimada, T., & Takagi, S. (2014). "Surface-fixation induced emission" of porphyrazine dye by a complexation with inorganic nanosheets. *Journal of Physical Chemistry C, 118*, 20466–20471.
42. Tokieda, D., Tsukamoto, T., Ishida, Y., Ichihara, H., Shimada, T., & Takagi, S. (2017). Unique fluorescence behavior of dyes on the clay minerals surface: Surface fixation induced emission (S-FIE). *Journal of Photochemistry and Photobiology A: Chemistry, 339*, 67–79.
43. Kudo, N., Tsukamoto, T., Shimada, T., & Takagi, S. (2018). Fluorescence enhancement behavior of hemicyanine derivatives on the clay nanosheets: Aggregation induced emission (AIE) vs. surface-fixation induced emission (S-FIE). *Chemistry Letters, 47*, 636–639.
44. Nakazato, R., Sano, K., Ichihara, H., Ishida, T., Shimada, T., & Takagi, S. (2019). Factors for the emission enhancement of dimidium in specific media such as in DNA and on a clay surface. *Physical Chemistry Chemical Physics: PCCP, 21*, 22732–22739.
45. Yoshida, Y., Shimada, T., Ishida, T., & Takagi, S. (2021). Effects of the surface charge density of clay minerals on surface-fixation induced emission of acridinium derivatives. *ACS Omega, 6*, 21702–21708.
46. Mei, J., Leung, N. L. C., Kwok, R. T. K., Lam, J. W. Y., & Tang, B. Z. (2015). Aggregation-induced emission: Together we shine, united we soar! *Chemical Reviews, 115*, 11718–11940. and references therein.
47. Mei, J., Hong, Y., Lam, J. W. Y., Qin, A., Tang, Y., & Tang, B. Z. (2014). Aggregation-induced emission: The whole is more brilliant than the parts. *Advanced Materials, 26*, 5429–5479.
48. Hirose, M., Ito, F., Shimada, T., Takagi, S., Sasai, R., & Okada, T. (2017). Photoluminescence by intercalation of a fluorescent β-diketone dye into a layered silicate. *Langmuir, 33*, 13515–13521.
49. Shimizu, M., Tatsumi, H., Mochida, K., Shimono, K., & Hiyama, T. (2009). Synthesis, crystal structure, and photophysical properties of (1E,3E,5E)-1,3,4,6-tetraarylhexa-1,3,5-trienes: A new class of fluorophores exhibiting aggregation-induced emission. *Chemistry—An Asian Journal, 4*, 1289–1297.
50. Kokado, K., Tokoro, K., & Chujo, Y. (2009). Luminescent and axially chiral π-conjugated polymers linked by carboranes in the main chain. *Macromolecules, 42*, 9238–9242.
51. Miyajima, R., Ooe, Y., Miura, T., Ikoma, T., Iwamoto, H., Takizawa, S., & Hasegawa, E. (2023). Triarylamine-substituted benzimidazoliums as electron donor-acceptor dyad-type photocatalysts for reductive organic transformations. *Journal of the American Chemical Society, 145*, 10236–10248.
52. Eguchi, M., Takagi, S., Tachibana, H., & Inoue, H. (2004). The 'size matching rule' in di-, tri-, and tetra-cationic charged porphyrin/synthetic clay complexes: Effect of the inter-charge distance and the number of charged sites. *Journal of Physics and Chemistry of Solids, 65*, 403–407.
53. Kuykendall, V. G., & Thomas, J. K. (1990). Photophysical investigation of the degree of dispersion of aqueous colloidal clay. *Langmuir, 6*, 1350–1356.
54. Chernia, Z., & Gill, D. (1999). Flattening of TMPyP adsorbed on laponite. Evidence in observed and calculated UV-vis spectra. *Langmuir, 15*, 1625–1633.
55. Fujimura, T., Shimada, T., Sasai, R., & Takagi, S. (2018). optical humidity sensing using transparent hybrid composed of cationic magnesium porphyrin and clay mineral. *Langmuir, 34*, 3572–3577.
56. Tsukamoto, T., Shimada, T., & Takagi, S. (2015). Structure resembling effect of clay surface on photochemical properties of meso-phenyl or pyridyl-substituted monocationic antimony(V) porphyrin derivatives. *RSC Advances, 5*, 8479–8485.